Full paper/Mémoire

Effect of phosphorus on the performance of IM-5 for the alkylation of toluene with methanol into *p*-xylene

Cui Wang, Yaquan Wang[*], Hengbao Chen, Xiao Wang, Hongyao Li, Chao Sun, Liying Sun, Chunyang Fan, Xu Zhang

Key Laboratory for Green Chemical Technology of Ministry of Education, School of Chemical Engineering & Technology, Tianjin University, Tianjin 300072, PR China

ABSTRACT

IM-5 zeolite was modified with different amounts of phosphorus species. The effect of the introduction of phosphorus into IM-5 zeolite (P-IM-5) was evaluated on the alkylation of toluene with methanol. The samples were characterized by X-ray diffraction, scanning electron microscopy, N_2 physical adsorption, ^{31}P magic angle spinning nuclear magnetic resonance, inductively coupled plasma optical emission spectroscopy, temperature-programmed desorption of ammonia, Fourier transform infrared spectra of pyridine, 2,6-di-*tert*-butyl-pyridine and 2,6-lutidine adsorption, and thermogravimetric analysis after reaction. The results showed that the zeolite structure was not changed, but the total amount of acid sites decreased with increasing phosphorus loading. The phosphorus-modified IM-5 samples exhibited much higher stability on the alkylation of toluene with methanol than the parent zeolite and the optimal phosphorus amount added was 0.5 wt %. The excellent catalytic performance could be ascribed to the low ratio of B/L acid sites upon phosphorus modification, which suppressed coke formation.

© 2018 Académie des sciences. Published by Elsevier Masson SAS. All rights reserved.

1. Introduction

para-Xylene is an important monomer in the synthesis of high purity terephthalic acid and dimethyl terephthalate, both of which are essential components to produce poly-ethylene terephthalate [1]. In recent years, the global de-mand of *p*-xylene has increased dramatically. Industrially, mobil selective toluene disproportionation process and isomerization of mixed xylene isomers are popular com-mercial methods for producing *p*-xylene [2]. However, benzene as a coproduct in these processes is inevitably present, and the relatively high cost of product purification makes it less attractive [3]. Thus, another economical route of *p*-xylene production, the alkylation of toluene with methanol, has attracted great attention. In this route, *p*-

xylene is the major product and a full utilization of toluene can be achieved with less byproducts. Besides, this route has the advantage of using methanol as the alkylating agent, which is cheap and available in abundance [4].

A variety of zeolites have been used to catalyze the alkylation of toluene with methanol. Among these zeolites, H-ZSM-5 shows good catalytic properties because of its three-dimensional (3D) pore structure and proper pore diameter [5,6]. In the previous exploration, scientists have been able to make the *p*-xylene selectivity reach more than 90% by modifying H-ZSM-5 with Si [7,8], P [9,10], B [11], Pt [12,13], Mg [14,15], and optimizing the process variables of the reaction [16,17]. Although a high selectivity to *p*-xylene can be obtained by traditionally impregnating with metal or nonmetal oxide, this method tends to suffer from an appreciable loss of the catalyst activity and stability because of partially blocked pore openings and signifi-cantly decreased acid sites [18]. Besides, the alkylation of

* Corresponding author.
  E-mail address: yqwang@tju.edu.cn (Y. Wang).

toluene with methanol reaction is accompanied by many side reactions. For instance, apart from the alkylation with toluene, methanol undergoes a secondary dehydration and immediately forms ethylene, which tends to become coke precursors on catalysts. Besides, large molecules such as polyaromatic can easily block pores and thus results in deactivation through carbon deposition [19].

Various modification measures have been taken to improve the catalyst activity with long-term stability. Sotelo et al. [20] studied the deactivation kinetics of toluene alkylation with methanol over Mg-modified ZSM-5 catalyst and found that the shape selectivity of the Mg-modified ZSM-5 is decreased by the coke deposition within the zeolite channels. Dakka et al. [21] reported that the modification of Rh improved the stability of silicon passivated ZSM-5. The selectivity to *p*-xylene reached 90% with the conversion of toluene almost stayed constant after 300 h on stream. Zhao et al. [22] investigated the effect of metal modification on the catalytic performance. They found that Si-P-Mg−modified ZSM-5 catalysts loading with metals having good hydrogenation properties, such as Pt, Pd, Co, and Ni, exhibit remarkable stability with high toluene conversion and selectivity to *p*-xylene. Janardhan et al. [23] reported the generation of new acid sites in phosphate-modified ZSM-5, which effectively catalyzed the alkylation of toluene. Faramawy et al. [24] improved the catalytic activity and stability while retaining the high *para*-selectivity by additional treatments of P-ZSM-5 with chromium and nickel. Wang et al. [25] synthesized a H-ZSM-5@S-1 catalyst with epitaxial growing a S-1 layer over HZSM-5 crystals. The catalyst showed high toluene conversion without apparent deactivation after 130 h on stream. However, the toluene conversion on ZSM-5 catalysts investigated is generally less than 30% and the operation steps are usually complex and difficult to control. Therefore, there is still a long way to go to develop a catalyst with long-term stability, high activity, and high *para*-selectivity.

In recent years, a novel zeolite, IM-5, was synthesized using 1,5-bis(*N*-methylpyrrolidinium) pentane bromide as a structure directing agent (SDA) [26−28]. Baerlocher et al. [29] categorized the topological structure of IM-5 to IMF (Institut français du pétrole and University of Mulhouse - five) using the charge-flipping structure analysis method. The structure of IM-5 is intersectional 2D 10-MR channel system with large internal 3D cavities, which is similar to that of ZSM-5. The IM-5 zeolite with distinctive pore structure, which can accommodate bulky intermediates, is considered as a promising catalyst [30,31]. The catalytic performance of IM-5 zeolite has been investigated in shape selective catalysis [32,33], nonoxidative aromatization [34,35], and selective catalytic reduction of nitric oxides [36−40] as well as the alkylation of toluene with methanol [41,42]. Chen et al. [41] synthesized a series of IM-5 zeolites modified with different amounts of phosphorus species from 3 to 8 wt %. The toluene conversion decreased from 50% on H-IM-5 to 22% on P-8%/IM-5, whereas the selectivity to xylene increased from 72% on H-IM-5 to 84% on P-8%/IM-5 and the selectivity to *p*-xylene slightly increased from 22% on H-IM-5 to 28% on P-8%/IM-5. The stability of P-modified IM-5 samples was not mentioned. The micropore

volume, mesopore volume, and the amounts of strong acid sites on P-IM-5 zeolite all decreased with the increase of phosphorus loadings. Chen et al. [42] reported that IM-5 exhibited higher catalytic activity and xylene selectivity than ZSM-5 in alkylation of toluene with methanol. After steam treatment, the activity of IM-5 decreased, but the selectivity to xylene increased. He et al. [43] made the first attempt to describe the framework Al substitutions, location, and strength of Brønsted acid of IM-5 using the density functional theory calculations. According to the calculations, there are about 40 preferable Al, H locations with relatively high acidity in IM-5 zeolite, which may rationalize why IM-5 is more active than ZSM-5 in catalysis reactions.

In this work, we modified IM-5 zeolite with different amounts of phosphorus species at much lower levels than the work of Chen et al. [41]. It was found that an appropriate amount of phosphorus at much low levels decreased the amounts of acid sites, especially the Brønsted acid sites, which effectively suppressed the formation of coke and extended the catalytic life without sacrificing the selectivity to xylene and *p*-xylene.

2. Experiment section

2.1. Materials

Sodium hydroxide (NaOH, AR) and methanol (analytical reagent (AR)) were purchased from Tianjin Guangfu Fine Chemical Research Institute Co., Ltd. Aluminum nitrate nonahydrate ($Al(NO_3)_3 \cdot 9H_2O$, AR) was obtained from Tianjin Kemiou Chemical Reagent Co., Ltd. Silica sol (40 wt % suspension in water) was purchased from Qingdao Haiyang Chemical Co., Ltd. Phosphoric acid (H_3PO_4, 85 wt %) was purchased from Li An Long Bohua Pharmaceutical Chemical Co., Ltd. Ammonium nitrate (NH_4NO_3, AR) was purchased from Guangdong Xilong Chemical Co., Ltd. Toluene was purchased from Tianjin Jiangtian Chemical Co., Ltd. 1,5-Bis(*N*-methylpyrrolidinium) pentane in its dibromide form ($1,5-MPPBr_2$) was purchased from Guangzhou Dayou Fine Chemical Co., Ltd. Commercial H-ZSM-5 zeolite ($SiO_2/Al_2O_3 = 50$) was purchased from the Catalyst Plant of Nankai University.

2.2. Synthesis of H-IM-5

The synthesis of zeolite IM-5 was carried out using $1,5-MPPBr_2$ as an SDA. Calculated amounts of $Al(NO_3)_3 \cdot 9H_2O$, distilled water, and NaOH were mixed together with stirring. When the solution became clear, $1,5-MPPBr_2$ was gradually added under vigorous stirring. Then, silica sol was added dropwise. The molar composition of the final mixture was $30SiO_2:0.75Al_2O_3:11Na_2O:1200H_2O:4.5R$, where R is $1,5-MPPBr_2$. After vigorously stirring at room temperature for 4 h, the synthesis mixture was transferred into Teflon-lined autoclaves and heated to 170 °C under rotation (30 rpm) for 8 days. The products were centrifuged and washed with distilled water until the pH reached about 7, dried at 120 °C for 12 h, and calcined in air at 550 °C for 6 h to remove the organic SDA. H-IM-5 was obtained through ion exchange with 1 M NH_4NO_3 solution for three

times at 80 °C, followed by drying at 120 °C for 12 h, calcination in air at 550 °C for 6 h.

2.3. Preparation of phosphorus-modified IM-5 zeolite

The phosphorus-modified IM-5 zeolites were prepared by incipient wetness impregnation of H-IM-5 with aqueous solutions of phosphoric acid at room temperature. Water was removed by evaporation at 120 °C for 10 h, and then the zeolite was calcined in flowing air at 550 °C for 1 h. The obtained samples are denoted as P-x/IM-5, where x represented the mass fraction of P to zeolite (x = 0.1%, 0.25%, 0.5%, 0.75%, and 2%, respectively).

2.4. Catalyst characterization

X-ray diffraction (XRD) patterns were obtained at room temperature using a Rigaku D/max 2500 diffractometer with Cu Kα radiation (λ = 0.1542 nm) and a scanning rate of 8°min^{-1} in the 2θ ranges from 5° to 40°.

Scanning electron microscopy (SEM) images were obtained using an S-4800 field emission SEM with an accelerating voltage of 3 kV to determine the size and morphology of the primary crystals and aggregates.

Nitrogen adsorption and desorption isotherms of the samples were measured at liquid N$_2$ temperature (77 K) using a Micromeritics TriStar 3000 automated physisorption instrument. All of the samples were degassed at 300 °C for 4 h before the measurements. The total specific surface area (S_{BET}) was derived from the Brunauer–Emmett–Teller (BET) equation. The external surface area (S_{ext}) was derived from the t-plot method, and the micropore surface area (S_{micro}) was calculated by subtracting S_{ext} from S_{BET}. The total pore volume (V_{total}) was obtained from the absorption amounts calculated at p/p_0 = 0.99. The micropore volume (V_{micro}) was also derived from the t-plot method, and the mesopore volume (V_{meso}) was calculated by subtracting V_{micro} from V_{total}.

Solid-state magic angle spinning nuclear magnetic resonance (MAS NMR) was performed on a Varian infinity plus 300 MHz NMR spectrometer equipped with a field strength of 7.1 T. ^{31}P MAS NMR spectra were recorded at 121.372 MHz at a spinning frequency of 10 kHz and 30 s intervals between successive accumulations. The chemical shifts were reported relative to 75% H$_3$PO$_4$. The deactivated sample was calcined at 550 °C to remove the deposited carbon before ^{31}P MAS NMR spectra measurement.

Temperature-programmed desorption of ammonia (NH$_3$-TPD) measurements were recorded using a TP-5076 chemical adsorption instrument (Xianquan Industrial and Trading Co., Ltd). One hundred milligrams of zeolite was pretreated in a helium flow at 400 °C for 1 h, cooled down to 100 °C, and then ammonia was introduced with helium as the carrier gas. After purging for 120 min, the flow was switched to helium and heated to 700 °C at a rate of 10 °C min^{-1}. The desorbed ammonia was monitored by a thermal conductivity detector.

The phosphorus content and SiO$_2$/Al$_2$O$_3$ ratio in zeolites were determined by an inductively coupled plasma optical emission spectroscopy (ICP-OES) using a Varian Vista-MPX emission spectrometer.

The Fourier transform infrared (FTIR) spectra of pyridine adsorption were recorded in the range of 1000–4000 cm^{-1} with a resolution of 4 cm^{-1} using a Bruker Vertex 70 spectrometer. Thirty-two milligrams of each sample was pressed into a self-supporting wafer, mounted inside a Pyrex vacuum cell, and degassed at 400 °C for 1 h to remove moisture and impurities. Samples were allowed to cool down to 60 °C, and then 4 μL pyridine vapor was admitted into the cell and adsorption lasted for 0.5 h. Subsequently, the samples were heated up to 200 °C under vacuum for spectrum recording. Similarly, the FTIR spectra of 2,6-di-tert-butyl-pyridine and 2,6-lutidine adsorption were obtained by the same method as mentioned previously.

Carbon deposition after reaction was evaluated by thermogravimetric analysis (TGA) with a Shimadzu TGA-50 instrument. The samples were combusted from room temperature to 750 °C with a heating rate of 10 °C min^{-1} in oxygen.

2.5. Catalytic tests

The catalytic reaction of toluene alkylation with methanol was carried out in a continuous flow fixed bed reactor with an internal diameter of 10 mm at 460 °C under atmospheric pressure. In a typical run, the catalyst particles with 20–40 mesh were obtained with a compression method. Catalyst (0.5 g) diluted with 2.0 g of quartz particles of the same sizes was loaded in the middle zone of the reactor. The temperature of the catalyst bed during the reaction was measured using a thermocouple that reached the middle of the reactor. The catalyst was activated in the flow of 50 mL min^{-1} N$_2$ at 460 °C for 1 h before reaction and then a mixture of toluene and methanol (T/M molar ratio = 2:1) was pumped into the reactor at a weight hourly space velocity (WHSV) of 2 h^{-1} by a micropump. The exit products were separated into gas, liquid hydrocarbons, and water using an ice-cooled condenser. The gas fractions were analyzed using a gas chromatograph (GCSP-3420A) equipped with a flame ionization detector and a KB-PLOTQ (50 m × 0.32 mm × 10.00 μm) capillary column. The liquid hydrocarbons were analyzed using a gas chromatograph (GCSP-3420A) equipped with a flame ionization detector and a SE-54 (30 m × 0.25 mm × 0.33 μm) capillary column. The toluene conversion and product selectivity were calculated by the following equations:

$$p\text{-xylene selectivity } (\%) = \frac{p\text{-xylene}}{p\text{-xylene} + o\text{-xylene} + m\text{-xylene}} \times 100$$

$$\text{Toluene conversion } (\%) = \frac{N_{\text{T,in}} - N_{\text{T,out}}}{N_{\text{T,in}}} \times 100$$

where N is the number of moles. Subscripts in and out represent the inlet and outlet of the reactor, respectively.

3. Results and discussion

3.1. Catalyst characterization

Fig. 1 shows the powder XRD patterns of H-IM-5 and P-modified IM-5 zeolites. All of the samples exhibit typical characteristic patterns of the IMF topology with peaks observed in the 2θ range of 5°–30° [44] without other impurity crystal phase observed. Moreover, no distinct peaks for phosphorus are detected in the P-modified samples, implying that phosphorus particles are highly dispersed or the amount of the phosphorus is too low to be detected. However, the crystallinity of P-modified IM-5 zeolites decreased slightly compared with H-IM-5, which is most likely owing to the framework defects caused by the introduction of phosphorus species [45,46].

Fig. 2 displays the SEM images of H-IM-5 and P-modified IM-5 zeolites. The SEM micrographs clearly indicate that all of the samples exhibit rod-like crystals around 200–300 nm in diameter, which is in good agreement with that of Ref. [47]. Moreover, no amorphous material is found, which also proves the high crystallinity of all the samples. Phosphorus modification does not change the morphology of IM-5.

The N_2 adsorption–desorption isotherms of H-IM-5 and P-modified IM-5 samples are shown in Fig. 3, and the corresponding data are summarized in Table 1. Obviously, H-IM-5 and the samples with different phosphorus content in the range of 0.12 wt % present the combination characteristic of type I and type IV isotherms with a closed hysteresis loop at high relative pressure ($p/p_o > 0.9$), implying that the mesopores are mainly intergranular pores generated by the accumulation of nanocrystals [48,49]. The H-IM-5 sample possesses large specific surface area of 367 cm^2 g^{-1} and

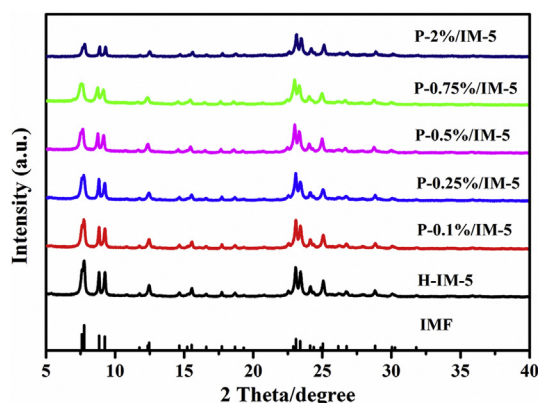micropore surface area of 314 cm^2 g^{-1}. At low level loadings of phosphorus (e.g., <0.5 wt %), the specific surface area, micropore surface area, total pore volume, and mesopore volume all are not changed appreciably. However, at high level loadings of phosphorus, especially at 2 wt % or greater, these values all decrease to a great extent. Obviously, high level loadings of phosphorus species cause the partial blockage of the zeolite pores.

Fig. S1 shows the ^{31}P MAS NMR spectra of H-IM-5 and P-modified IM-5 catalysts. For the P-modified IM-5 catalysts, several peaks appeared to be in the 0 to −40 ppm region. The intensities of all these peaks increased with the increase of phosphorus loadings. The peak at −7.0 ppm is attributed to phosphorus in pyrophosphoric acid, pyrophosphates, or terminal groups in short-chain polyphosphates, whereas the −16.0 ppm signal is related to intermediate groups in short-chain polyphosphates or pyrophosphates [50,51]. The signal at −30.1 ppm is assigned to amorphous aluminum phosphate [52], and the signals in the −30 to −40 ppm region are attributed to $(SiO)_xAl(OP)_{4-x}$ species [53], These results are in good agreement with N_2 adsorption–desorption results, indicating the presence of aluminum phosphate and polyphosphate chains blocking the pore channels.

The phosphorus content and SiO_2/Al_2O_3 ratios of the synthesized samples determined by ICP-OES are also listed in Table 1. There are no much differences in the SiO_2/Al_2O_3 ratios. The phosphorus content is consistent with the amount of phosphorus added during the impregnation.

The NH_3-TPD profiles of H-IM-5 and P-modified IM-5 samples are shown in Fig. 4. All of the samples show a typical NH_3-TPD spectrum with two peaks at the low and high temperatures, corresponding to weak and strong acid sites, respectively. There are no much differences among the peak temperatures of both the low and high temperature peaks on each sample. The results demonstrate that the introduction of phosphorus species does not change the strength of both the weak acid and the strong acid. The acid amounts obtained from NH_3-TPD profiles are summarized in Table 2. It is seen that the introduction of phosphorus species has a significant effect on the concentration of acid sites: the concentrations of both the strong acid sites and the weak acid sites decrease with the increase of phosphorus loadings, especially the concentrations of the strong acid sites decrease to a larger extent. When the phosphorus loadings are lower than 0.5 wt %, the amount of the strong acid sites sharply decreases from 0.459 mmol g^{-1} on H-IM-5 to 0.242 mmol g^{-1} on P-0.5%/IM-5, whereas further increasing the phosphorus loadings to 2 wt % only results in a slight decrease to 0.196 mmol g^{-1}. It is generally accepted that the strong acid sites favor various side reactions such as toluene disproportionation, which leads to the formation of coke, i.e., polyaromatics [54]. Hence, the decreased concentration of strong acid sites of P-modified IM-5 catalysts is expected to improve the catalytic performance in the alkylation of toluene with methanol reaction.

The external surface acidity of H-IM-5 and P-modified IM-5 samples was investigated using FTIR spectroscopy with 2,6-di-tert-butyl-pyridine (DTBPy) as a probe molecule. The spectra of all the samples are shown in Fig. S2. Infrared spectra of DTBPy adsorbed on all of the samples
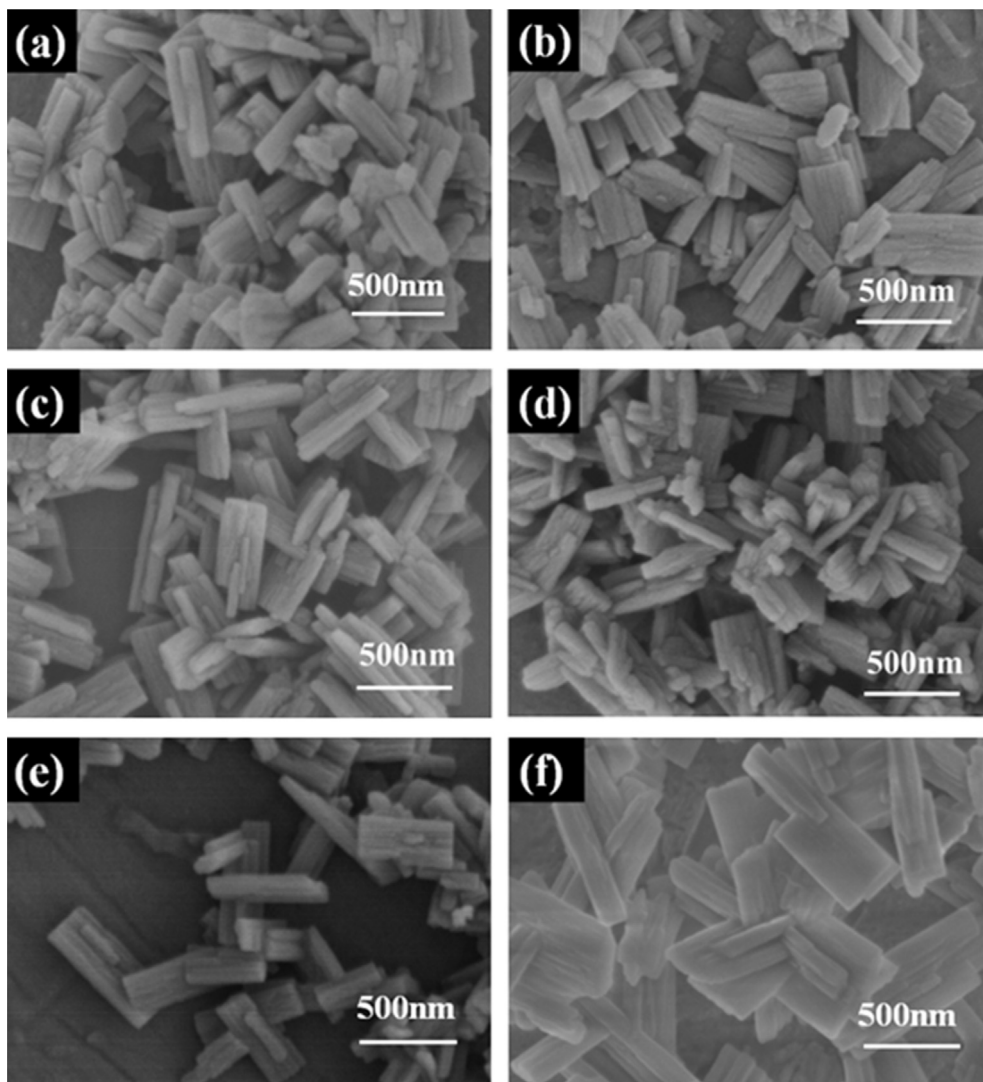

Fig. 1. XRD patterns of H-IM-5 and P-x% (x = 0.1, 0.25, 0.5, 0.75, 2)/IM-5 catalysts.

Fig. 2. SEM images of (a) H-IM-5, (b) P-0.1%/IM-5, (c) P-0.25%/IM-5, (d) P-0.5%/IM-5, (e) P-0.75%/IM-5, and (f) P-2%/IM-5.
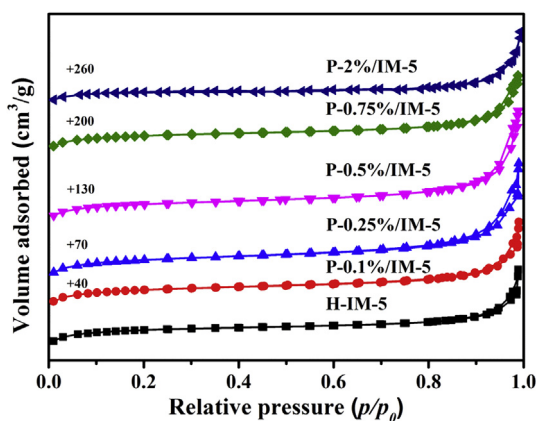

Fig. 3. N$_2$ adsorption−desorption isotherms of H-IM-5 and P-x% (x = 0.1, 0.25, 0.5, 0.75, 2)/IM-5 catalysts.

show a broad band located around 2956 cm^{-1}, which is assigned to the asymmetric stretching vibration of the −CH$_3$ groups in DTBPy, indicating the existence of a hydrogen bonding between the −CH$_3$ groups and the hydroxyl groups of the zeolite [55,56]. With the increase of phosphorus loadings to 0.5 wt %, the intensity of −CH$_3$ groups in DTBPy is slightly reduced while further increasing of phosphorus loadings to 2 wt % results in a significant decrease, indicating that part of the acid sites on the external surface was passivated under high phosphorus loadings.
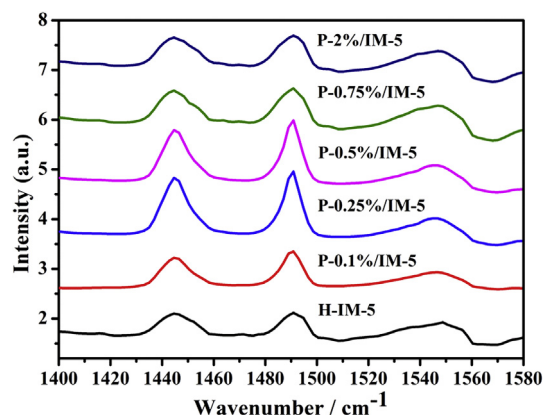
The acidity of H-IM-5 and P-modified IM-5 samples was further investigated using FTIR spectroscopy with pyridine as a probe molecule (Py-IR). The Py-IR spectra of all the samples are shown in Fig. 5. The absorption peaks at 1545 and 1445 cm^{-1} are assigned to the pyridine molecule adsorbed on Brønsted (B) and Lewis (L) acid sites, respectively, whereas the absorption peak at 1490 cm^{-1} is

Table 1
Textural properties of the H-IM-5 and P-x% (x = 0.1, 0.25, 0.5, 0.75, 2)/IM-5 catalysts.

Catalysts	SiO$_2$/Al$_2$O$_3$ ratios[a]	P content (wt %)[a]	Surface area (m^2 g^{-1})			Pore volume (cm^3 g^{-1})		
			S_{BET}[b]	S_{ext}[c]	S_{micro}[c]	V_{total}[d]	V_{micro}[e]	V_{meso}[e]
H-IM-5	26	–	367	53	314	0.247	0.146	0.101
P-0.1%/IM-5	25	0.14	367	58	309	0.239	0.144	0.095
P-0.25%/IM-5	29	0.22	366	67	299	0.223	0.139	0.084
P-0.5%/IM-5	29	0.45	348	60	288	0.215	0.133	0.082
P-0.75%/IM-5	27	0.72	338	52	286	0.207	0.133	0.074
P-2%/IM-5	28	1.96	280	45	235	0.176	0.114	0.062

[a] Determined by ICP-OES.
[b] Derived from the BET equation.
[c] S_{ext} was derived from the t-plot method, S_{micro} was calculated by subtracting S_{ext} from S_{BET}.
[d] Calculated at $p/p_o = 0.99$.
[e] V_{micro} was evaluated by the t-plot method, V_{meso} was calculated by subtracting V_{micro} from V_{total}.

Fig. 4. NH$_3$-TPD profiles of H-IM-5 and P-x% (x = 0.1, 0.25, 0.5, 0.75, 2)/IM-5 catalysts.
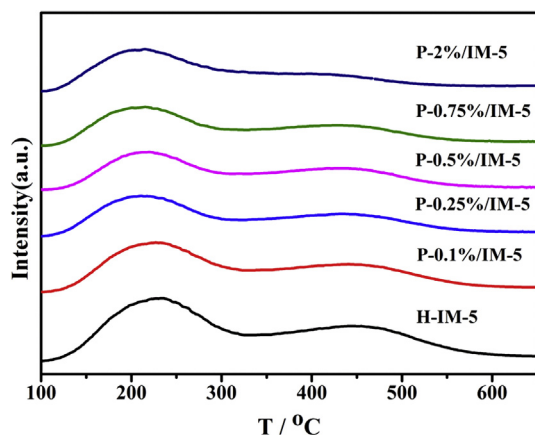
Fig. 5. Py-IR spectra of H-IM-5 and P-x% (x = 0.1, 0.25, 0.5, 0.75, 2)/IM-5 catalysts.

attributed to the combination of B and L acid sites. The ratios of B/L are obtained according to the corresponding extinction coefficient of B and L acid sites [57] and the results are also listed in Table 2. Here, the ratio of B/L is taken as a parameter to investigate the changes in the relative amounts of B and L acid sites with different phosphorus loadings. It was reported that the incorporation of phosphorus into IM-5 zeolite led to a sharp decrease in the concentration of both B and L acid sites [58], which was also found in this work. Because of the steric hindrance induced by the methyl group, 2,6-lutidine is a more sensitive probe

of B acid sites than pyridine and preferentially adsorbed on B acid sites even in the presence of strong L acid sites, thus acts as a good probe adsorbate for the B acid sites [59–63]. The spectra of all the samples are shown in Fig. S3. Infrared spectra of 2,6-lutidine adsorbed on all the samples show a broad band located around 1643 cm^{-1}, which is assigned to the 2,6-lutidine protonated on B acid sites [64]. There is no obvious peak of 2,6-lutidine adsorbed on L acid sites. It is seen that the introduction of phosphorus species does effect the concentration of B acid sites: the concentration of B acid sites decreases with the increase of phosphorus loadings. It is well known that the production of a B acid site is

Table 2
Acid amounts integrated from NH$_3$-TPD profiles of H-IM-5 and P-x% (x = 0.1, 0.25, 0.5, 0.75, 2)/IM-5 catalysts.

Catalysts	Total acidity (mmol g^{-1})	Weak acidity (mmol g^{-1})	Strong acidity (mmol g^{-1})	B/L[a]
H-IM-5	1.601	1.142	0.459	1.28
P-0.1%/IM-5	1.304	0.949	0.355	0.76
P-0.25%/IM-5	1.076	0.791	0.285	0.65
P-0.5%/IM-5	0.941	0.699	0.242	0.61
P-0.75%/IM-5	0.865	0.647	0.218	1.18
P-2%/IM-5	0.814	0.618	0.196	1.28

[a] C (pyridine on B sites) $= \varepsilon_B \times I_B \times \dfrac{R^2}{W}$, C (pyridine on L sites) $= \varepsilon_L \times I_L \times \dfrac{R^2}{W}$

$\varepsilon_B = 1.67$ cm/μmol, $\varepsilon_L = 2.22$ cm/μmol

B/L $= 1.67/2.22 \times I_B/I_L$.

attributed to the substitution of a Si atom by an Al atom in the framework of zeolites, and the L acid site was coordinative unsaturated Al^{3+}. Thus, the amount of framework Al is proportional to the concentration of both B and L acid sites [65,66]. Seo and Ryoo [67] and Zhuang et al. [68] all reported the formation of octahedral aluminum through the interaction of framework aluminum with phosphorus species. Caro et al. [69] reported that the introduction of phosphorus decreased the concentration of B acid sites, which is caused by the reaction of H_3PO_4 with the Brønsted OH groups of H-ZSM-5 zeolite. The interaction between phosphorus species with framework aluminum results in the decreased concentration of B and L acid sites. As shown in Table 2, when the phosphorus content is lower than 0.5 wt %, the ratio of B/L decreases with the increase in phosphorus content, which can be attributed to the more reduction of B acid sites than L acid sites, whereas further increase of phosphorus loadings results in an increase in the ratio of B/L, which is mainly caused by the significant decrease of L acid sites. Overall, with increasing phosphorus loading, the total acid sites decrease, which is consistent with the NH_3-TPD results, but the ratio of B/L presents a first decrease and then an increase tendency with the minimum on P-0.5%/IM-5 catalyst.

3.2. Catalytic performance in alkylation of toluene with methanol

Xylene selectivity and *p*-xylene selectivity are presented as a function of time on stream for H-IM-5 and P-modified IM-5 catalysts in Fig. 6. Chen et al. [41] investigated the change in the selectivity to xylene under a relatively high level of phosphorus loadings (3−8 wt %). They reported that the selectivity to xylene increased from 72% on H-IM-5 to 84% on P-8%/IM-5. In this work, low level loadings of phosphorus (<0.5 wt %) did not have a significant effect on the selectivity to xylene. The selectivity to xylene on P-modified samples is almost the same as that of H-IM-5 when the phosphorus content is lower than 0.5 wt %. Further increasing phosphorus content to 2 wt % results in a slight increase. This is mainly because of the elimination of strong acid sites covered by phosphorus species, which could effectively restrain the side reactions such as toluene
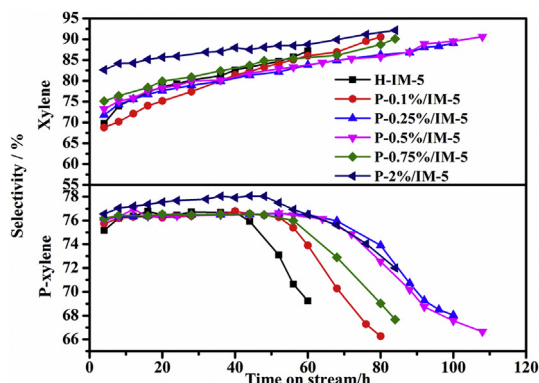
disproportionation. With the reaction on stream the selectivity to xylene increases and can also reach the values reported by Chen et al. [41].

The selectivity to *p*-xylene for all catalysts is very stable, but drops appreciably after the late stage of reaction on stream, which is obviously caused by coke deposition inside the channels of the zeolite, making the reaction only occurring on outside of the surface and losing shape selectivity to the zeolite. There are no appreciable differences in the selectivity to *p*-xylene on H-IM-5 and low level phosphorus loading samples (0.1, 0.25, 0.5, and 0.75 wt %), which is around 76%. Further increasing phosphorus content to 2 wt % only results in a slight increase of 2%. It could be concluded that low level loadings of phosphorus (<0.5 wt %) did not have a significant effect on the selectivity to xylene and *p*-xylene.

Fig. 7 shows the effect of phosphorus addition on the toluene conversion on H-IM-5, P-modified IM-5, and H-ZSM-5 zeolites in the alkylation of toluene with methanol. The catalyst lifetime here is denoted as the reaction time from the beginning to the time when the conversion of toluene dropped less than 25% and the reaction was stopped after the deactivation. As shown in Fig. 7, the initial toluene conversion on H-IM-5 is slightly higher than those on P-modified IM-5 catalysts. However, H-IM-5 deactivates fast. With the addition of phosphorus, the catalysts deactivate much slowly, with the catalytic lifetime increasing from 58 to 102 h with the increase of phosphorus loadings to 0.5 wt %. But a further increase of phosphorus loadings to 2 wt % results in the decrease of lifetime (66 h), which can be attributed to diffusional barriers of reactants and products within the pores, thus leading to quick deactivation [70]. It is generally accepted that the alkylation reaction happens mainly on the weak B acid sites within the pores of the zeolites [9,71]. Besides, the low density of B/L acid sites can enhance the toluene methylation reaction to produce *p*-xylene, whereas the high density of B/L acid sites favors the various side reactions such as further alkylation of xylene, which are responsible for the rapid deactivation by coking [7,72,73]. The P-0.5%/IM-5 catalyst, which possesses the minimum ratio of B/L, exhibits the longest catalytic lifetime
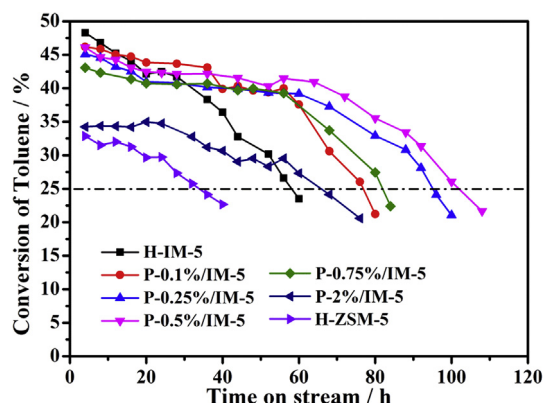

Fig. 6. Xylene selectivity and *p*-xylene selectivity on H-IM-5 and P-*x*% (*x* = 0.1, 0.25, 0.5, 0.75, 2)/IM-5 catalysts.

Fig. 7. Toluene conversion on H-IM-5, P-*x*% (*x* = 0.1, 0.25, 0.5, 0.75, 2)/IM-5 and H-ZSM-5 catalysts. Reaction conditions: 460 °C; 0.1 MPa; 0.5 g zeolite; WHSV = 2 h^{-1}; *n* (toluene)/*n* (methanol) = 2:1; carrier gas: high purity N_2, 60 mL min^{-1}. Testing was stopped at around 25% toluene conversion.
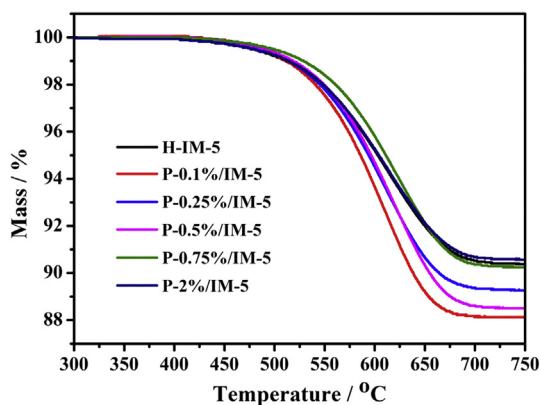
Fig. 8. Thermogravimetric curves of deactivated H-IM-5 and P-*x*% (*x* = 0.1, 0.25, 0.5, 0.75, 2)/IM-5 catalysts in alkylation of toluene with methanol.
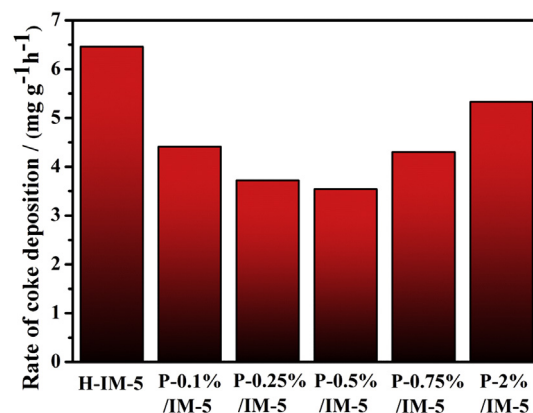

Fig. 9. Carbon deposition rates on H-IM-5 and P-*x*% (*x* = 0.1, 0.25, 0.5, 0.75, 2)/IM-5 catalysts in alkylation of toluene with methanol.

of 102 h on stream and excellent catalytic performance in toluene methylation reaction with a toluene conversion of 41.5% and *p*-xylene selectivity of 83.3% after 56 h on stream.

The performance of a commercial H-ZSM-5 (SiO_2/Al_2O_3 = 50) catalyst was also investigated. As depicted in Fig. 6, it only runs 32 h before the conversion of toluene decreases to 25% and the maximum conversion of toluene is 34%, both of which are much lower than those of the H-IM-5 and the P-modified IM-5 samples.

The deactivated P-0.5%/IM-5 sample is denoted as D-P-0.5%/IM-5. Fig. S4 shows the ^{31}P MAS NMR spectra of H-IM-5, P-0.5%/IM-5, and D-P-0.5%/IM-5 catalysts. For both the P-0.5%/IM-5 and D-P-0.5%/IM-5 catalysts, several peaks appeared in the 0 to −40 ppm region. The peak at −7.0 ppm is attributed to phosphorus in pyrophosphoric acid, pyrophosphates, or terminal groups in short-chain polyphosphates, whereas the −16.0 ppm signal is related to intermediate groups in short-chain polyphosphates or pyrophosphates [50,51]. The signal at −30.1 ppm is assigned to amorphous aluminum phosphate [52], and the signals in the −30 to −40 ppm region are attributed to $(SiO)_xAl(OP)_{4−x}$ species [53]. Compared with the P-0.5%/IM-5 catalyst, the intensities of the peaks of D-P-0.5%/IM-5 catalyst at −7.0 and −16.0 ppm decrease whereas those at −30.1 ppm and in the −30 to −40 ppm region are not changed significantly after the reaction. These results indicate that not all the phosphorus species retained in the zeolites during catalysis because of the high reaction temperature and phosphorus mainly exists in the form of aluminum phosphate after the reaction.

The deactivated catalysts were further investigated using TGA to obtain the carbon deposition information and the results are depicted in Fig. 8. The mass loss of the catalysts over the temperature range of 300−750 °C reflects the decomposition of the coke deposited on the deactivated zeolites. The deactivation of catalyst in the alkylation of toluene with methanol is mainly caused by carbonaceous residues such as large molecules formed via polymerization of ethylene or aromatics, which could block the pores of catalysts and cover the acid sites, thus consequently leads to deactivation [13]. The coke amounts occurred in P-modified catalysts is higher than that of H-IM-5 when the

phosphorus loading is less than 0.5 wt %, owing to the longer lifetime of the P-modified catalysts. The rates of coke deposition for all catalysts are calculated by the amount of coke deposited divided by the reaction time and the results are shown in Fig. 9. With phosphorus modification at low levels (<0.5 wt %), the rate of coke deposition is much lower than that of the parent H-IM-5. It has been reported that B acid sites are active centers not only for alkylation but also for coke formation [66]. As shown by pyridine adsorption, at low levels (<0.5 wt %) of phosphorus modification, the ratio of B/L decreases with increasing amounts of phosphorus species. This might be the reason why rate of coke deposition also decreases with the minimum occurred at 0.5 wt %. Further increasing the phosphorus amount to high levels (>0.75 wt %), the ratio of B/L increases and therefore, the rate of coke deposition increases. It can be concluded that the addition of low level phosphorus species can optimize the acid type of the P-modified IM-5 catalysts to achieve the minimum ratio of B/L acid sites, thereby weakening the tendency of coke formation rate and extend the catalytic lifetime.

4. Conclusions

IM-5 zeolite was modified with different amounts of phosphorus species. The effect of phosphorus modification was studied for the alkylation of toluene with methanol. Phosphorus modification led to partial elimination of the total acid sites without causing obvious damage to the IMF structure. Phosphorus modification at low levels (less than 0.5 wt %) also led to the decrease of the Brønsted acid sites to a larger extent than that of the Lewis acid sites. It might be such an effect of phosphorus modification that suppressed coke formation in the alkylation of toluene with methanol, and therefore significantly extended the catalytic lifetime without sacrificing the selectivity to xylene and *p*-xylene.

Appendix A. Supplementary data

Supplementary data to this article can be found online at https://doi.org/10.1016/j.crci.2018.11.005.

References

[1] W.W. Kaeding, C. Chu, L.B. Young, B. Weinstein, S.A. Butter, J. Catal. 67 (1981) 159.
[2] W. Alabi, L. Atanda, R. Jermy, S. Al-Khattaf, Chem. Eng. J. 195 (2012) 276.
[3] H. Wu, M. Liu, W. Tan, K. Hou, A. Zhang, Y. Wang, X. Guo, J. Energy Chem. 23 (2014) 491.
[4] A.B. Halgeri, Bull. Catal. Soc. India 2 (2003) 184.
[5] S. Al-Khattaf, Ind. Eng. Chem. Res. 46 (2007) 59.
[6] N.Y. Chen, Ind. Eng. Chem. Res. 40 (2001) 4157.
[7] P. Lu, Z. Fei, L. Li, X. Feng, W. Ji, W. Ding, Y. Chen, W. Yang, Z. Xie, Appl. Catal., A 453 (2013) 302.
[8] S. Zheng, H.R. Heydenrych, A.A. Jentys, J.A. Lercher, J. Phys. Chem. B 106 (2002) 9552.
[9] M. Ghiaci, A. Abbaspur, M. Arshadi, B. Aghabarari, Appl. Catal., A 316 (2007) 32.
[10] S. Cavallaro, L. Pino, P. Tsiakaras, N. Giordano, B.S. Rao, Zeolites 7 (1987) 408.
[11] M.B. Sayed, J.-C. Védrine, J. Catal. 101 (1986) 43.
[12] A.K. Aboul-Gheit, S.M. Abdel-Hamid, E.A. Emam, Appl. Catal., A 179 (1999) 107.
[13] Y. Zhao, W. Tan, H. Wu, A. Zhang, M. Liu, G. Li, X. Wang, C. Song, X. Guo, Catal. Today 160 (2011) 179.
[14] T. Yashima, Y. Sakaguchi, S. Namba, Stud. Surf. Sci. Catal. 7 (1981) 739.
[15] Y.G. Li, W.H. Xie, S. Yong, Appl. Catal., A 150 (1997) 231.
[16] J.P. Breen, R. Burch, M. Kulkarni, D. McLaughlin, P.J. Collier, S.E. Golunski, Appl. Catal., A 316 (2007) 53.
[17] J.P. Breen, R. Burch, M. Kulkarni, P.J. Collier, S.E. Golunski, J. Am. Chem. Soc. 127 (2005) 5020.
[18] W.W. Kaeding, C. Chu, L.B. Young, S.A. Butter, J. Catal. 69 (1981) 392.
[19] M.A. Uguina, D.P. Serrano, R.V. Grieken, S. Vènes, Appl. Catal., A 99 (1993) 97.
[20] J.L. Sotelo, M.A. Uguina, J.L. Valverde, D.P. Serrano, Ind. Eng. Chem. Res. 35 (1993) 2548.
[21] J.M. Dakka, J.S. Buchanan, R.A. Crane, C.N. Elia, X. Feng, L.L. Iaccino, G.D. Mohr, B.A. Raich, J.G. Santiesteban, L. Zhang. US Patent 7,453,018, 2010.
[22] Y. Zhao, H. Wu, W. Tan, M. Zhang, M. Liu, C. Song, X. Wang, X. Guo, Catal. Today 156 (2010) 69.
[23] H.L. Janardhan, G.V. Shanbhag, A.B. Halgeri, Appl. Catal., A 471 (2014) 12.
[24] S. Faramawy, S.M. El-Sabagh, N.Y. Al-Mehbad, React. Kinet. Catal. Lett. 66 (1999) 257.
[25] C.F. Wang, Q. Zhang, Y.F. Zhu, D.K. Zhang, J.Y. Chen, F.K. Chiang, Mol. Catal. 433 (2017) 242.
[26] E. Benazzi, H. Cauffriez. Dealuminated IM-5 zeolite, US Patent 5,968,475 (1999).
[27] E. Benazzi, N. George-Marchal, C. Gueret, P. Briot, A. Billon, P. Marion. US Patent 5,989,410 (1999).
[28] E. Benazzi, J.L. Guth, L. Rouleau, US Patent 6,136,290 (2000).
[29] C. Baerlocher, F. Gramm, L. Massüger, L.B. Mccusker, Z. He, S. Hovmöller, X. Zou, Science 315 (2007) 1113.
[30] L. Wang, W. Yang, C. Xin, F. Ling, W. Sun, X. Fang, R. Yang, Mater. Lett. 69 (2012) 16.
[31] L. Wang, W. Yang, F. Ling, Z. Shen, R. Yang, W. Sun, X. Fang, H. Ji, Microporous Mesoporous Mater. 163 (2012) 243.
[32] A. Corma, J.N. Martínez-Triguero, S. Valencia, E. Benazzi, S. Lacombe, J. Catal. 206 (2002) 125.
[33] J. Jae, G.A. Tompsett, A.J. Foster, K.D. Hammond, S.M. Auerbach, R.F. Lobo, G.W. Huber, J. Catal. 279 (2011) 257.
[34] H. Liu, S. Wu, Y. Guo, F. Shang, X. Yu, Y. Ma, C. Xu, J. Guan, Q. Kan, Fuel 90 (2011) 1515.
[35] H. Liu, C. Zhou, Y.N. Zhang, Q.B. Kan, J. Fuel Chem. Technol. 45 (2017) 1074.
[36] A.E. Palomares, J.G. Prato, A. Corma, Ind. Eng. Chem. Res. 42 (2003) 1538.
[37] J.K. Lee, Y.J. Kim, H.J. Lee, S.H. Kim, S.J. Cho, I.S. Nam, S.B. Hong, J. Catal. 284 (2011) 23.
[38] P.N.R. Vennestrøm, T.V.W. Janssens, A. Kustov, M. Grill, A. Puig-Molina, L.F. Lundegaard, R.R. Tiruvalam, P. Concepción, A. Corma, J. Catal. 309 (2014) 477.
[39] A.E. Palomares, F. Márquez, S. Valencia, A. Corma, J. Mol. Catal., A 162 (2000) 175.
[40] N. He, H.B. Xie, Y.H. Ding, Microporous Mesoporous Mater. 121 (2009) 95.
[41] J. Chen, C. Zhang, Y. Wang, M. Sun, X. Mu, X. Shu, Acta Petrol. Sin. 29 (2013) 757.
[42] Q. Chen, Y. Wang, M. Sun, X. Mu, X. Shu, Acta Petrol. Sin. 26 (2010) 165.
[43] N. He, H.B. Xie, Y.H. Ding, Microporous Mesoporous Mater. 111 (2008) 551.
[44] A. Corma, A. Chica, J.M. Guil, F.J. Llopis, G. Mabilon, J.A. Perdigón-Melón, S. Valencia, J. Catal. 189 (2000) 382.
[45] Z. Song, A. Takahashi, I. Nakamura, T. Fujitani, Appl. Catal., A 384 (2010) 201.
[46] G. Zhao, J. Teng, Z. Xie, W. Jin, W. Yang, Q. Chen, Y. Tang, J. Catal. 248 (2007) 29.
[47] X. Ji, H. Jia, Y. Wang, X. Yang, J. Porous Mater. 1 (2018) 1.
[48] J.C. Groen, L.A. Peffer, J.A. Moulijn, J. Perez-Ramirez, Chemistry 11 (2005) 4983.
[49] H. Chen, Y. Wang, F. Meng, C. Sun, H. Li, Z. Wang, F. Gao, X. Wang, S. Wang, Microporous Mesoporous Mater. 244 (2017) 301.
[50] J. Caro, M. Bülow, M. Derewinski, J. Haber, M. Hunger, J. Kärger, H. Pfeifer, W. Storek, B. Zibrowius, J. Catal. 21 (1990) 367.
[51] G.ö. Hlmann, H.-G. Jerschkewitz, G. Lischke, R. Eckelt, B. Parlitz, E. Schreier, B. Zibrowius, E. LöFfler, Stud. Surf. Sci. Catal. 65 (1991) 1.
[52] P.M. Bautista, J.M. Campelo, A. Garcia, D. Luna, J.M. Marinas, A.A. Romero, Appl. Catal., A 96 (1993) 175.
[53] T. Blasco, A. Corma, J. Martineztriguero, J. Catal. 237 (2006) 267.
[54] L.D.T. Câmara, K. Rajagopal, D.A.G. Aranda, Stud. Surf. Sci. Catal. 139 (2001) 61.
[55] J. Lyu, H. Hu, C. Tait, J. Rui, C. Lou, Q. Wang, W. Han, Q. Zhang, Z. Pan, X. Li, Chin. J. Chem. Eng. 25 (2017) 1187.
[56] J. Dewing, G.T. Monks, B. Youll, J. Catal. 48 (1977) 440.
[57] C.A. Emeis, J. Catal. 141 (1993) 347.
[58] A. Corma, J. Mengual, P.J. Miguel, Appl. Catal., A 461 (2013) 106.
[59] V. Lebarbier, M. Houalla, T. Onfroy, Catal. Today 192 (2012) 123.
[60] S. Nair, A.H.M. Shahadat Hussain, B.J. Tatarchuk, Fuel 105 (2013) 695.
[61] H.A. Benesi, J. Catal. 28 (1973) 176.
[62] J. Macht, C.D. Baertsch, M. May-Lozano, S.L. Soled, Y. Wang, E. Iglesia, J. Catal. 227 (2004) 479.
[63] L. Oliviero, A. Vimont, J.-C. Lavalley, F. Romero Sarria, M. Gaillard, F. Maugé, Phys. Chem. Chem. Phys. 7 (2005) 1861.
[64] S.N. Timmiati, A.A. Jalil, S. Triwahyono, H.D. Setiabudi, N.H.R. Annuar, Appl. Catal., A 459 (2013) 8.
[65] H.L. Hu, J.H. Lyu, J.Y. Rui, J. Cen, Q.F. Zhang, Q.T. Wang, W.W. Han, X.N. Li, Catal. Sci. Technol. 6 (2016) 2647.
[66] L.H. Ong, M. Dömök, R. Olindo, A.C. van Veen, J.A. Lercher, Microporous Mesoporous Mater. 164 (2012) 9.
[67] G. Seo, R. Ryoo, J. Catal. 124 (1990) 224.
[68] J. Zhuang, D. Ma, G. Yang, Z. Yan, X. Liu, X. Liu, X. Han, X. Bao, P. Xie, Z. Liu, J. Catal. 228 (2004) 234.
[69] J. Caro, M. Bülow, M. Derewinski, M. Hunger, J. Kärger, U. Kürschner, H. Pfeifer, W. Storek, B. Zibrowius, Stud. Surf. Sci. Catal. 52 (1989) 295.
[70] J.H. Kim, T. Kunieda, M. Niwa, J. Catal. 173 (1998) 433.
[71] A. Borgna, J. Sepúlveda, S.I. Magni, C.R. Apesteguía, Appl. Catal., A 276 (2004) 207.
[72] L. Zhang, J. Gao, J. Hu, W. Li, J. Wang, Catal. Lett. 130 (2009) 355.
[73] Z. Zhu, Q. Chen, Z. Xie, W. Yang, C. Li, Microporous Mesoporous Mater. 88 (2006) 16.